



Microenergy acoustic pulses induced myogenesis of urethral striated muscle stem/progenitor cells

Kai Cui^{1,2}, Ning Kang¹, Lia Banie¹, Tie Zhou^{1,3}, Tianshu Liu¹, Bohan Wang¹, Yajun Ruan¹, Dongyi Peng¹, Hsun Shuan Wang¹, Tianyu Wang¹, Guifang Wang¹, Amanda B. Reed-Maldonado¹, Zhong Chen^{1,2}, Guiting Lin¹, Tom F. Lue¹

¹Knappe Molecular Urology Laboratory, Department of Urology, School of Medicine, University of California, San Francisco, CA, USA;

²Department of Urology, Tongji Hospital, Huazhong University of Science and Technology, Wuhan 430030, China; ³Department of Urology, Shanghai Changhai Hospital, The Second Military Medical University, Shanghai 200433, China

Contributions: (I) Conception and design: G Lin, TF Lue; (II) Administrative support: Z Chen, L Banie, G Lin, TF Lue; (III) Provision of study material or patients: K Cui, N Kang, G Lin, TF Lue; (IV) Collection and assembly of data: K Cui, N Kang, L Banie, T Zhou, T Liu, B Wang, Y Ruan, D Peng, HS Wang, T Wang, G Wang, G Lin; (V) Data analysis and interpretation: K Cui, N Kang, L Banie, AB Reed-Maldonado, G Lin; (VI) Manuscript writing: All authors; (VII) Final approval of manuscript: All authors.

Correspondence to: Tom F. Lue, MD, Department of Urology, University of California, San Francisco, 400 Parnassus Ave., Ste A-630, San Francisco, CA 94143-0738, USA. Email: Tom.lue@ucsf.edu.

Background: Stress urinary incontinence (SUI) is a common disorder with high prevalence in women across their life span, but there are no non-surgical curative options for the condition. Stem cell-based therapy, especially endogenous stem cell therapy may be a potential treatment method for SUI. The aims of this study are to identify, isolate, and assay the function of urethral striated muscle derived stem/progenitor cells (uMDSCs) and to assess uMDSC response to microenergy acoustic pulses (MAP).

Methods: Urethral striated muscle was identified utilizing 3D imaging of solvent organs (3DISCO) and immunofluorescence (IF). uMDSCs were isolated and purified from Zucker Lean (ZL) (ZUC-LEAN) (ZUC-Leprfa 186) rats, with magnetic-activated cell sorting (MACS) and pre-plating methods. The stemness and differentiation potential of the uMDSCs were measured by cell proliferation, EdU, flow cytometry, IF, and Western blot.

Results: Comparison of the cell proliferation assays between MACS and pre-plating reveals the advantage of MACS over pre-plating. In addition, the study reveals that uMDSCs form myotubes when treated with MAP.

Conclusions: The uMDSCs within female rat urethral striated muscle could be a therapeutic target of MAP in managing SUI.

Keywords: Stress urinary incontinence (SUI); urethral striated muscle derived stem/progenitor cells (uMDSCs); microenergy acoustic pulses (MAP); Zucker Lean (ZL) rats; myogenesis

Submitted Mar 21, 2019. Accepted for publication Aug 14, 2019.

doi: 10.21037/tau.2019.08.18

View this article at: <http://dx.doi.org/10.21037/tau.2019.08.18>

Introduction

Urinary incontinence (UI), characterized by involuntary leakage of urine, is a common disorder affecting the life quality of approximately 50% of American women (1). UI can be classified into stress UI (SUI), urge UI (UUI), and

mixed UI (MUI), which has elements of both SUI and UUI (2). SUI, defined as a “complaint of involuntary loss of urine on effort or physical exertion, or sneezing or coughing”, is the most common type of incontinence, affecting 50–86% of female UI patients (3).

The urethral sphincter, which relies on the mechanical

integrity of striated and smooth muscle cells (SMCs), is implicated in female SUI (4). A previous study reported that the stress continence control system consists of two anatomical parts: the urethral support system and the sphincteric closure system (5). The urethral support system includes the anterior vagina, endopelvic fascia, arcus tendineus fasciae pelvis, and levator ani muscles. It provides a supportive layer upon which the urethra rests (5). The sphincteric closure system includes the urethral striated muscles, urethral smooth muscle, and vascular elements (6). Dysfunction of the sphincteric closure system is directly associated with female SUI. Conservative therapeutic options for women with SUI include behavioral modification, lifestyle modification, and pharmacotherapy, while these treatments are usually unsatisfactory (7). The most common surgical options for female SUI, the mid-urethral synthetic sling, may also have significant complications despite its high efficacy (8). Therefore, the regeneration-competent urethra striated muscle cells might become an alternative treatment method if the cells can be identified, isolated, purified, and activated to function.

Several studies have reported that SUI can be improved with the use of stem cells isolated from skeletal muscle (9), adipose tissue (10), bone marrow (11) and umbilical cord blood cells (12). Among these tissue types, skeletal muscle is a form of striated muscle consisting of myofibers. Myofibers are composed of mesoderm progenitors, which originate from the satellites cells (3). Many studies have demonstrated the importance of satellites cells in muscle regeneration and recovery (13), but there are few studies investigating the use of urethral striated muscle stem cells. Our previous study found that urethral muscle-derived stem/progenitor cells (uMDSCs) can be isolated successfully and can form myotubes *in vitro* (3). In this study, we aimed to demonstrate the isolation, purification, and function of uMDSCs in hopes of clearly defining urethral anatomy and further advance research utilizing stem cell-based treatments for SUI.

Low-intensity extracorporeal shock wave therapy (LiESWT) is used currently to treat musculoskeletal disorders such as tendinopathies and bone defects (14). Recent studies have reported that LiESWT may stimulate regeneration of skeletal muscle tissue and accelerate the muscle repair process (15). We have developed a similar but better technology microenergy acoustic pulses (MAP), which consists of a single predominantly positive pressure pulse followed by a relatively larger stretched wave component. Compared to standard shock wave, the MAP has a lower peak pressure (up to 21.8 MPa), slower pressure

risers (5 ms), and longer duration (~15 ms).

To clearly show the potential value of uMDSCs in the treatment of SUI, we located, isolated, and characterized uMDSCs in the whole urethra of Zucker Lean (ZL) (ZUC-LEAN) (ZUC-Leprfa 186) rats female rats. In addition, we also explored the function of uMDSCs and defined the specific biological effect of MAP.

Methods

Animals

Ten ZL female rats at 12-week-old were used in this experiment. All rats were obtained from Charles River Laboratories (Wilmington, MA, USA). Rats were housed and cared for according to guidelines of the Institutional Animal Care and Use Committee (IACUC) of University of California, San Francisco. All efforts were taken to minimize animal suffering and minimize the number of animals used.

Tissue 3D imaging of solvent-cleared organs (3DISCO)

Rats were anesthetized with isoflurane and sacrificed by thoracotomy. After euthanasia, the rat urethras were harvested *en bloc* with the anterior vaginal wall and fixed in cold 2% formaldehyde and 0.002% saturated picric acid in 0.1 M phosphate buffered saline (PBS), pH 8.0 for 4 h followed by overnight immersion in 0.1M PBS containing 30% sucrose. 3DISCO was conducted as previously reported (16). In brief, the whole urethra was harvested and immediately prepared in PBS buffer containing 1% Triton X-100 for 48 h. Then, it was incubated with primary antibodies: anti α -smooth muscle actin (SMA; 1:1,000; Abcam, UK) and muscle heavy chain (MHC; 1:1,000; Abcam, UK) in PBS containing 0.2% Triton X-100, 5% fetal bovine serum (FBS), and 2% bovine serum albumin (BSA) for another 48 h. This was followed by washing in PBS containing 0.2% Triton X-100 overnight. After incubation with secondary antibodies (1:500; Alexa Fluor-conjugated goat anti rabbit and mouse antibodies, Invitrogen, Carlsbad, USA) in PBS containing 0.2% Triton X-100, 5% FBS, and 2% BSA for 48 h, it was again washed in PBS containing 0.2% Triton X-100 overnight. Finally, the tissue clearing protocol was performed using 50% tetrahydrofuran (THF) for 30 min, 80% THF for 30 min, 100% THF for 30 min 3 times, 100% dichloromethane (DCM) for 20 min, and 100% benzyl ether for 30 min. After processing the tissue

was colorless and suitable for scanning.

Immunofluorescence (IF)

Sections of urethra samples were prepared according to the previous report (17). Tissues were incubated with primary antibodies: anti α -SMA (1:500; Abcam), MHC, (1:500; Abcam), Paired Box 7 (Pax7; 1:500; Santa Cruz Bio, USA), Sex determining region Y-box 2 (Sox2), and Lin28. Secondary antibodies included Alexa Fluor-conjugated goat anti rabbit and mouse antibodies (1:500; Invitrogen). The muscle was also stained with Alexa-488-conjugated phalloidin (1:500; Invitrogen).

Tissue sections were also prepared as report in our previous study (3). These sections were incubated with primary antibodies: anti MHC (1: 500, Abcam). After washing with PBS three times, the cells were incubated with Alexa Fluor-conjugated goat anti-rabbit antibody (1:500; Invitrogen) for 1 hour at room temperature. After washing with PBS again, these cells were stained with 4',6-diamidino-2-phenylindole (DAPI; for nuclear staining, 1 μ g/mL, Invitrogen). In addition, these cells were assessed for EdU labeling using the Click-iT reaction cocktail (Invitrogen), which contained Alexa Fluor 594 (1:500), for 30 min at room temperature.

Finally, these tissues and cell sections were photographed and recorded using a Retiga Q Image digital still camera and ACT-1 software (Nikon Instruments Inc., Melville, NY, USA) for image analysis.

Isolation of female urethral striated muscle stem cells

ZL female rats were used for isolating uMDSCs. First, the whole urethra was harvested and cut into 1 mm³ pieces and digested in enzymatic dissociation containing 0.2% collagen II (Invitrogen) for 90 min with vigorous shaking. Then, the suspension was filtered through a 70 μ m nylon filter (Falcon) to obtain the cells.

Isolating uMDSCs^{MACS} with magnetic-activated cell sorting (MACS)

After washing with medium (DMEM containing 2% FBS, 1% Pen/Strep, 1% ascorbic acid) three times, the cell pellets were re-suspended in medium and incubated with the primary antibodies (anti CD31-Biotin and CD45-Biotin) for 30 min on ice. Anti-Biotin Microbeads (Miltenyi Biotec, Auburn, CA, USA) were then added to the cell suspension and incubated for another 30 min on ice. The

cell mixture was washed with MACS buffer twice, re-suspended in MACS buffer, and loaded into the magnetic column (Miltenyi Biotec) pre-equilibrated with 2 mL MACS buffer. We obtained the target CD31⁺CD45⁻ cells for further isolation. For the second purification, the cell mixture was incubated for 30 min with primary antibodies: anti CD34⁻Biotin (Chemicon) and Integrin α 7-Biotin (Miltenyi Biotec) for 30 min on ice, followed by the incubation with goat anti-mouse IgG Microbeads (Miltenyi Biotec). After washing with MACS buffer twice again, the cells were re-suspended with MACS buffer, and loaded into the magnetic column pre-equilibrated with 2 mL MACS buffer. Finally, we obtained the (CD31⁻, CD45⁻) CD34⁺ Integrin α 7⁺ cells. The cells were then cultured in DMEM containing 20% FBS, 1% Pen/Strep, and 1% ascorbic acid. Cell viability was assessed with LIVE/DEAD[®] Fixable Dead Cell Stain Kits (Life Technologies, Grand Island, NY). The isolated cells were labeled "uMDSCs^{MACS}" and used in the 5–10th passage.

Isolating uMDSCs^{PP} with the pre-plating method

The pre-plating technique is based on the differential adherence characteristics of primary culture cells to a gelatin-coated surface. The filtered cell pellets were re-suspended in regular medium (DMEM containing 20% FBS, 1% Pen/Strep, 1% ascorbic acid) and subsequently pre-cultured onto a 10 cm dish. According the previous report (18), the uMDSCs remained in the cellular supernatant and the other cells attached quickly to the bottom due to different adherence rates. The suspension was then transferred to another 10 cm dish after 48 h. After transferring 3 times, the remaining cells in the suspension were labeled "uMDSCs^{PP}".

Cell proliferation assay

For the determination of viable cell number, the uMDSCs^{MACS} and uMDSCs^{PP} were plated in 96-well plates at a density of ~1,000 cells/well in the experiment medium. After 24 and 72 h incubation, the number of viable cells, the cell proliferation rate, and the cell doubling time were determined using CellTiter 96[®] Non-Radioactive Cell Proliferation Assay (MTT) method according to the manufacturer's instruction.

Flow cytometry

We tested a series of cell surface markers according to our previous studies (3,19), including Int-7 α , CD56, CD34,

PAX7, Myf5 and CD105 (20,21). These uMDSCs^{MACS} and uMDSCs^{PP} from both methods were incubated with primary antibodies as described above in PBS with 1% FBS and 0.1% Na₃N for 30 min on ice. They were then incubated with Phycoerythrin (PE) conjugated secondary antibody, followed by washing in PBS with 1% FBS and 0.1% Na₃N twice. These cells were fixed in PBS with 1% paraformaldehyde and analyzed by a fluorescence-activated cell sorter (FACS Vantage SE System, BD Biosciences, San Jose, USA). Data were analyzed with FlowJo software (Tree Star, Inc., Ashland, USA).

Myotube formation

Both uMDSCs^{MACS} and uMDSCs^{PP} prepared with pre-plating and MACSs were seeded into 6-well plates for the myotube formation assay as previously reported (3,22), with L6 as the possible control. In brief, the cells were grouped into four: (I) Control group (Ctrl): cells treated with regular medium (DMEM containing 10% FBS, 1% Pen/Strep, 1% ascorbic acid); (II) Induction group (Ind): cells treated with 2% horse serum; (III) MAP group: cells treated with regular medium and MAP (0.02 mJ/mm², 2 Hz, 100 pulses) every 3 days for one week; (IV) Induction and MAP group (Ind + MAP): cells treated with 2% HS and MAP (0.02 mJ/mm², 2 Hz, 100 pulses) every 3 days for one week. All experiments were repeated in triplicate on cells from each subject.

Western blot

Cell protein samples were harvested as reported previously (3). Equal amounts of protein samples (30 µg per lane) were electrophoresed in sodium dodecyl sulfate polyacrylamide gel and then transferred to polyvinylidene difluoride membranes (Millipore Corp, Bedford, MA, USA). Membranes were blocked in the PBS with 5% BSA for 1 h, followed by the incubation with primary antibodies: MHC (1:1,000; Abcam), myogenin (MyoG; 1:1,000; Santa Cruz), and β-actin (1:500; Santa Cruz). After the incubation with secondary antibodies, the resulting images were analyzed with ChemiImager 4000 (Alpha Innotec) to determine the integrated density value of each protein band.

Statistics analysis

The images were quantified using Image-Pro Plus (Media Cybernetics, Silver Spring, MD, USA), and the data were analyzed using GraphPad Prism 5.0 (GraphPad Software,

San Diego, CA, USA) and expressed as means ± standard error of mean. Analysis of variance (one-way ANOVA) followed by paired *t*-test was used to determine differences between groups. Statistical significance was set at a P value less than 0.05.

Results

Location and distribution of striated muscle in the female rat external urethral sphincter

To clearly show the location and distribution of female urethral striated muscle in 3D, tissue 3DISCO was performed on the whole urethra. *Figure 1* shows the 3D image of the whole urethra from the proximal portion at the bladder neck through to the distal urethra and demonstrates the urethral smooth muscle (α-Actin in red) and urethral striated muscle (MHC in green). Moreover, the images reveal the detailed distribution of SMA and MHC in the upper and lower halves of the rat external urethral sphincter (*Figure 1B,C*). IF was performed to show the internal SMA layer and the external MHC layer of the urethra (*Figure 1D*). In addition, IF demonstrated the location of SMA and MHC in the cross-section of the mid-urethra, a longitudinal urethral section, and the longitudinal rear wall (*Figure S1*). This further demonstrates the organization and structure of the normal rat urethra.

Identification and isolation of uMDSCs

To localize muscle satellite cells within the urethral wall, IF was performed to determine the expression of cellular markers of satellite cells, including Pax7, Sox2, and Lin28. The utility of Pax7, a classical marker of muscle satellite cells, has been reported in our previous study (3). Sox2 is highly expressed in neural stem cells, and Lin28 is expressed in human embryonic stem cells (23,24). All of these markers are positive in uMDSCs (*Figure 2A*). Next, we isolated uMDSCs through MACS and pre-plating methods (*Figure 2B*) and labeled the cells as uMDSCs^{MACS} and uMDSCs^{PP}, respectively. We found that the yield of cells from MACS was significantly higher than that of pre-plating (*P*<0.05) (*Figure 2C*).

Cell proliferation assay of uMDSCs

Progenitor cells, or cells with stem properties, are characterized by the ability to retain nucleotide analogs, such as BrdU or EdU, for a prolonged period of time.

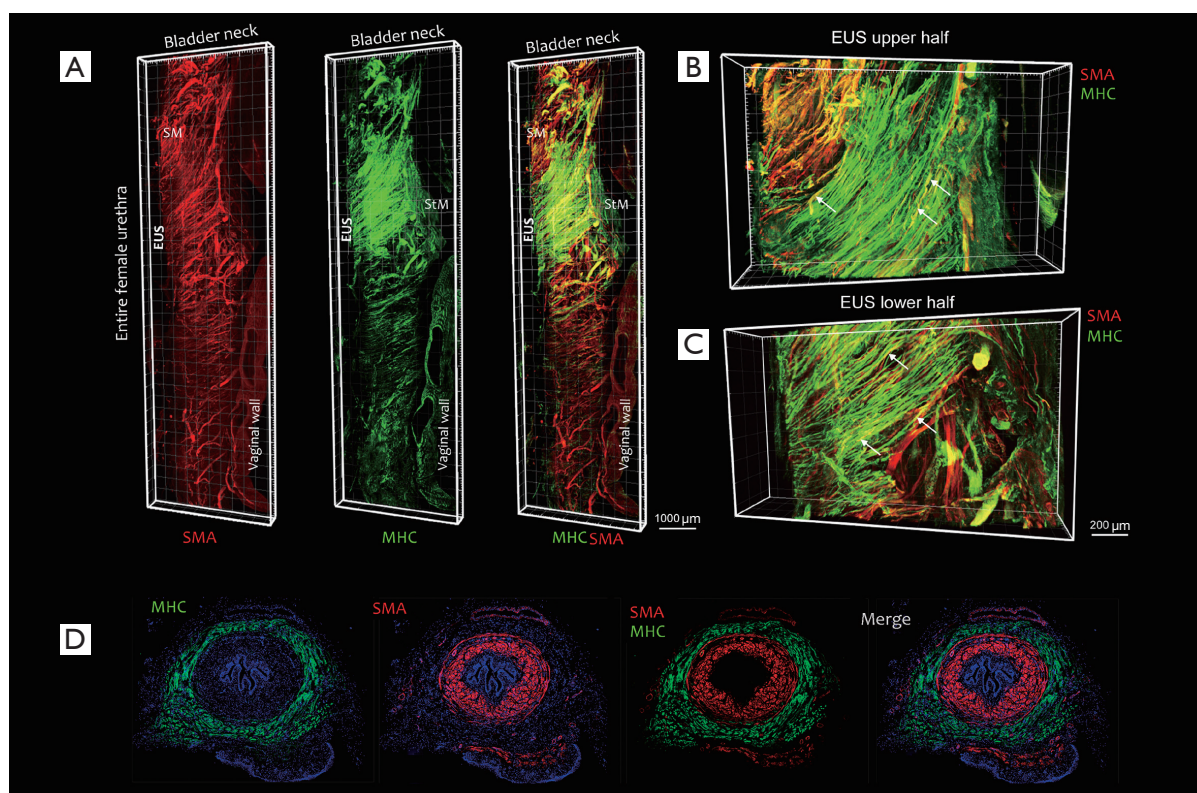


Figure 1 Location and distribution of striated muscle in the female external urethral sphincter. (A) 3DISCO image of the whole urethra from the proximal bladder neck to the distal urethra stained with SMA (red) and MHC (green); (B) 3DISCO image of the upper half of the external urethral sphincter stained with SMA (red) and MHC (green); (C) 3DISCO image of the lower half of the external urethral sphincter stained with SMA (red) and MHC (green); (D) representative images of the urethra stained with SMA (red) and MHC (green). EUS, external urethral sphincter; SMA, smooth muscle actin; MHC, muscle heavy chain; 3DISCO, 3D imaging of solvent organs.

Therefore, to compare the proliferation of uMDSCs between the two methods, we determined the EdU+ cells in uMDSCs^{MACS} and uMDSCs^{PP}. The total number of EdU+ cells in uMDSCs^{MACS} was significantly higher than in uMDSCs^{PP} ($P < 0.05$) (Figure 3A). We also performed the MTT method to test the proliferation of uMDSCs. The results revealed that at both 24 and 72 h uMDSCs^{MACS} had significantly more cells than uMDSCs^{PP} ($P < 0.05$) (Figure 3B,C). In addition, the cell proliferation rate and cell doubling time were also determined. Cell proliferation of uMDSCs^{MACS} was higher than that of uMDSCs^{PP}, and the cell doubling time of uMDSCs^{MACS} was shorter than that of uMDSCs^{PP}. These findings were consistent with the EdU result ($P < 0.05$) (Figure 3D,E).

FACS assay of uMDSCs

To ensure consistency, a small part of each P1 cell preparation

was tested by flow cytometry. The results indicated the expression of cell surface antigens in a pattern similar to most previous studies. The cellular markers were checked with FACS. It was noted that there were more Myf 5 (56.65%), CD34 (14.2%), CD105 (0.135%) in uMDSCs^{MACS} than in uMDSCs^{PP} [Myf 5 (40.85%), CD34 (11.4%), CD105 (0.06%)]. There were more PAX7 (0.484%) and CD56 (0.105%) in uMDSCs^{PP} than in uMDSCs^{MACS} [PAX7 (0.05%) and CD56 (0.088%)]. The expression of int-7a was similar between uMDSCs^{MACS} and uMDSCs^{PP}. Interestingly, the double staining of Int-7a/CD56, CD34/CD56, Myf5/PAX7, and Myf5/CD105 was much higher in uMDSCs^{PP} (0.057, 0.137, 24.7, and 36%, respectively) as compared to uMDSCs^{MACS} (0, 0.047, 14.5, and 28.3%, respectively).

Myotube formation of uMDSCs

To compare the differentiation ability of the uMDSCs from

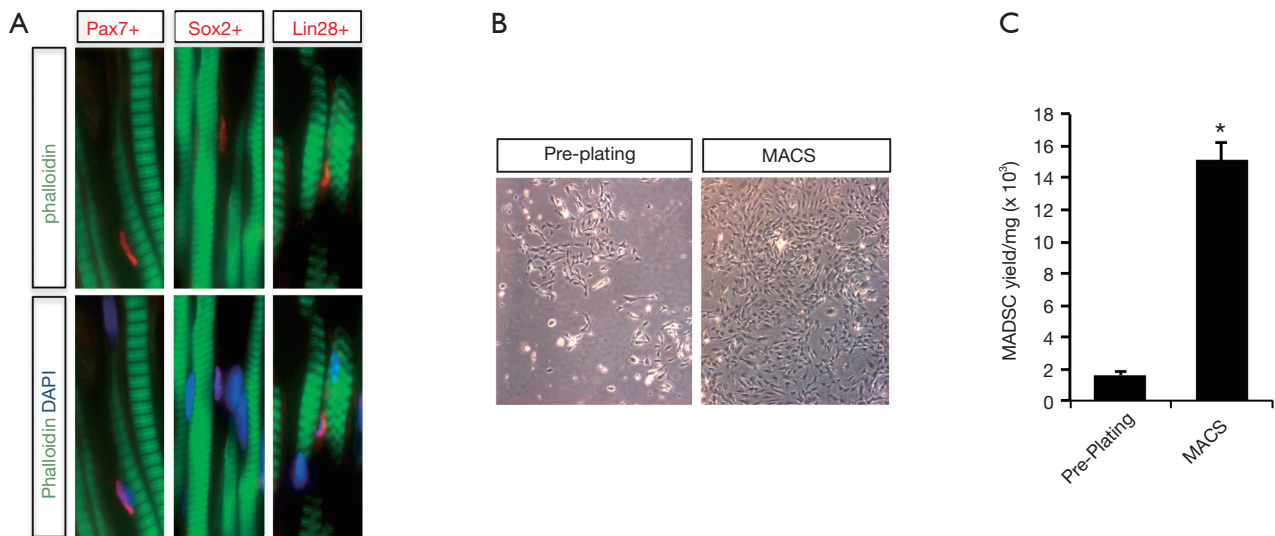


Figure 2 Identification and isolation of uMDSCs. (A) Identification of uMDSCs with Pax7, Sox2, and Lin28; $\times 1,000$. (B) representative image of fresh isolated uMDSCs through MACS and pre-plating methods. White light, $\times 50$; (C) the yield of cells from MACS and pre-plating methods. *, $P < 0.05$. Pax7, Paired Box 7; Sox2, Sex determining region Y-box 2; DAPI, 4',6-diamidino-2-phenylindole; MACS, magnetic-activated cell sorting; uMDSCs, urethral striated muscle derived stem/progenitor cells.

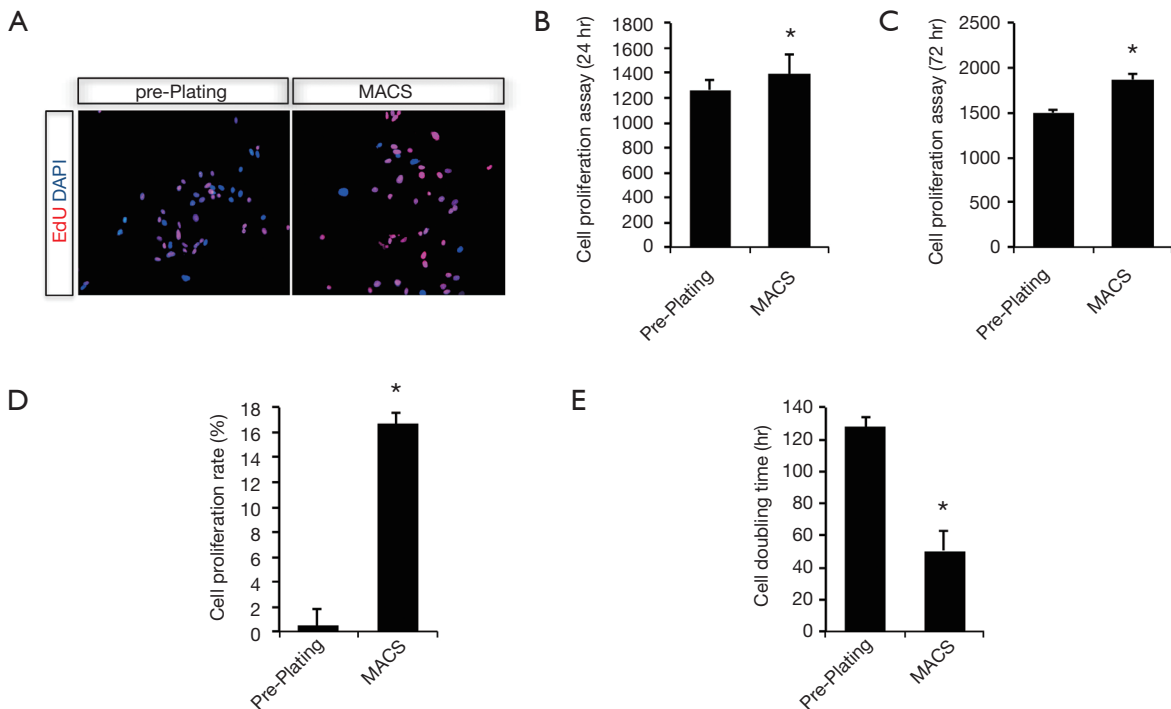


Figure 3 Cell proliferation assay of uMDSCs. (A) Representative images of EdU(+) cells (red) in uMDSCs^{MACS} and uMDSCs^{PP}. $\times 20$; (B) cell proliferation assay of uMDSCs^{MACS} and uMDSCs^{PP} at 24 h; (C) cell proliferation assay of uMDSCs^{MACS} and uMDSCs^{PP} at 72 h; (D) cell proliferation rate of uMDSCs^{MACS} and uMDSCs^{PP}; (E) cell doubling time of uMDSCs^{MACS} and uMDSCs^{PP}. *, $P < 0.05$. DAPI, 4',6-diamidino-2-phenylindole; MACS, magnetic-activated cell sorting; uMDSCs, urethral striated muscle derived stem/progenitor cells.

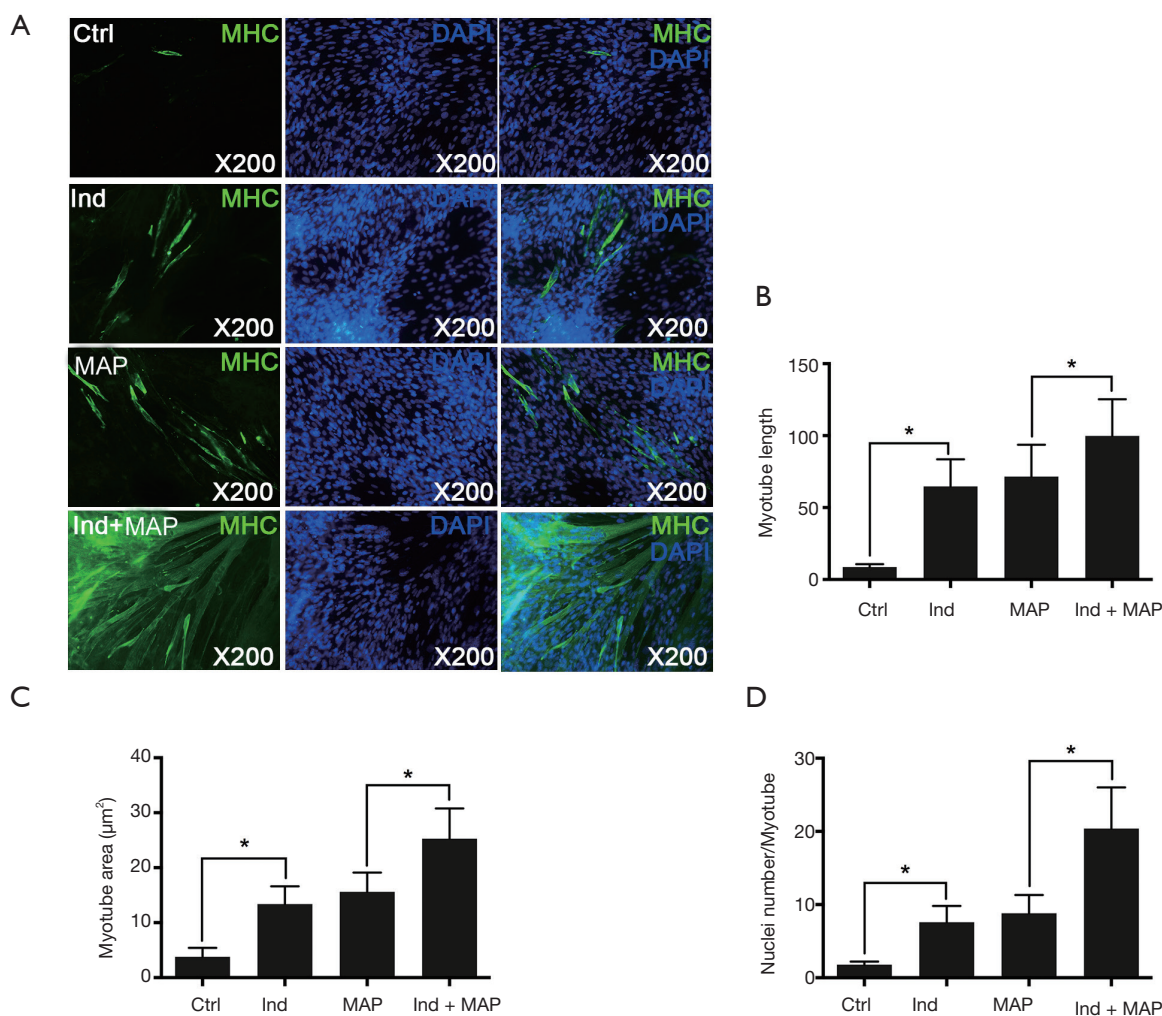


Figure 4 Myotube formation of uMDSCs^{MACS}. (A) Representative images of four groups in uMDSCs^{MACS} stained by MHC (green) and DAPI (blue), ×200; (B) average myotube length. The values are the means ± standard deviation for 300 myotubes in each group; (C) the average myotube area. The values are the means ± standard deviation for 300 myotubes in each group; (D) the average number of nuclei per myotube. The values are the means ± standard deviation for 100 myotubes in each group. *, P<0.05. Ctrl, Control group; Ind, Induction group; MAP, microenergy acoustic pulses group; MHC, muscle heavy chain; DAPI, 4',6-diamidino-2-phenylindole; MACS, magnetic-activated cell sorting; uMDSCs, urethral striated muscle derived stem/progenitor cells.

the two methods, we used induction medium (DMED containing 2% horse serum) to induce formation of myotubes, which can be stained by MHC. The myotube length, myotube area, and nuclei per myotube were determined. Compared to the Control group, the Ind group, MAP group, and Ind + MAP group showed longer, larger myotubes and more nuclei per myotube. The myotube length, myotube area, and nuclei per myotube were also greatly increased compared to the Ind group and MAP group (all P<0.05) (Figures 4,5). There was no obvious difference between Ind

group and MAP group. To further verify the differentiation of uMDSCs, we also determined the expression of MHC and MyoG proteins. Compared to the Ctrl group, the Ind group and MAP group both had increased expression of MHC and MyoG. Moreover, the Ind + MAP group showed higher expression of MHC and MyoG than the Ind group or the MAP group. This suggests a cooperative effect between the induction medium and MAP for induction of myotube formation (P<0.05) (Figure 6). The positive control L6 presented similar results (Figure S2).

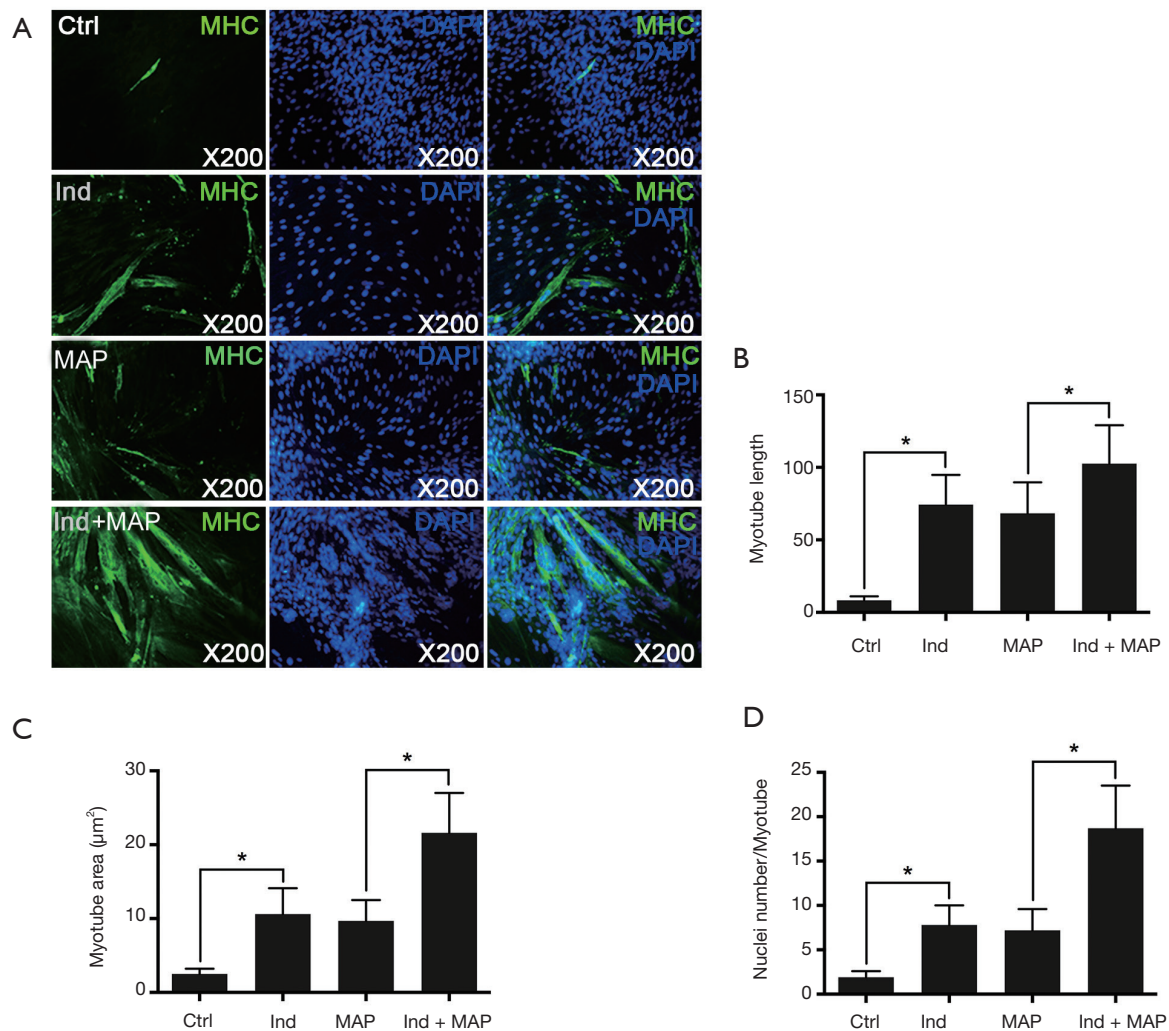


Figure 5 Myotube formation of uMDSCs^{PP}. (A) Representative images of four groups in uMDSCs^{PP} stained by MHC (green) and DAPI (blue), ×200; (B) average myotube length. The values are the means ± standard deviation for 300 myotubes in each group; (C) the average myotube area. The values are the means ± standard deviation for 300 myotubes in each group; (D) the average number of nuclei per myotube. The values are the means ± standard deviation for 100 myotubes in each group. *, P<0.05. Ctrl, Control group; Ind, Induction group; MAP, microenergy acoustic pulses group; MHC, muscle heavy chain; DAPI, 4',6-diamidino-2-phenylindole; uMDSCs, urethral striated muscle derived stem/progenitor cells.

Discussion

SUI is a common and chronic condition associated with a deficient urethral sphincter which is unable to generate enough closure pressure to resist increases in abdominal pressure during physical activity (2). Normal urethral sphincter function is predominantly based on the urethral striated muscle, smooth muscle, and vascular elements (22). It is well known that the female rat urethral musculature consists of an inner longitudinal smooth muscle layer, a

middle circular smooth muscle layer, and an outer striated muscle layer. The longitudinal smooth muscle is distributed along the entire length of the urethra and may actually be a continuation of the bladder smooth muscle. However, the striated muscle is confined to the proximal half of the structure similar to the urethra in women (25).

In the present study, we describe the distribution of rat urethral muscle with both 3DISCO and IF. The examination of tissue histology by light microscopy is a fundamental tool for investigating the structure and

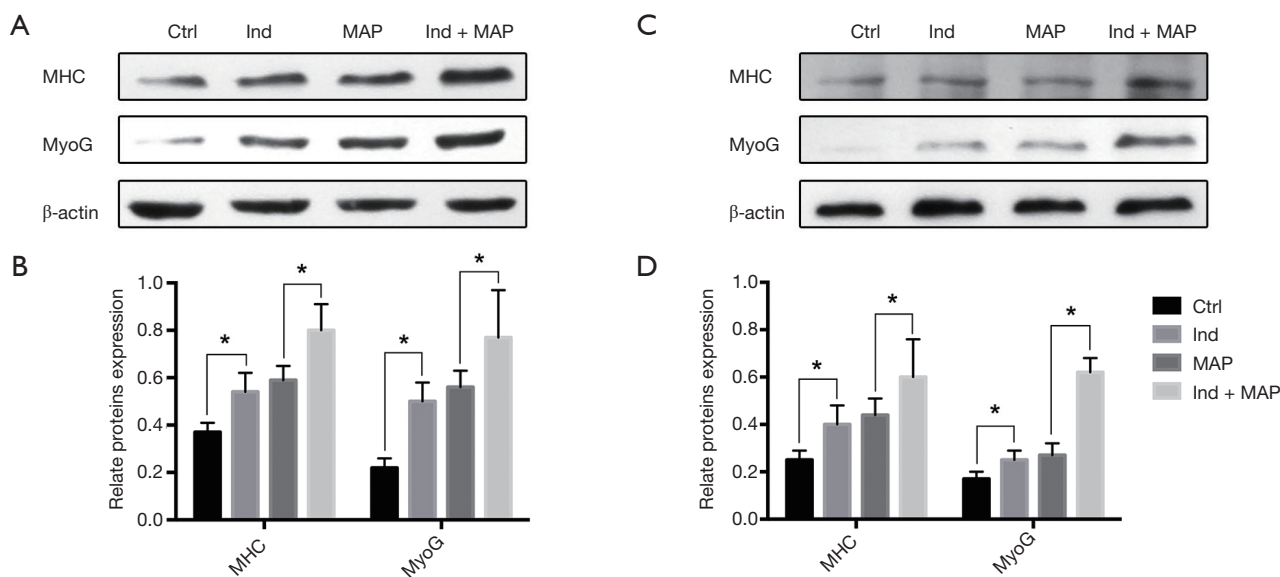


Figure 6 Myotube formation of uMDSCs assayed with Western blot. (A) Representative western blot results of MHC and MyoG of all four groups in uMDSCs^{MACS}; (B) the expression level of MHC and MyoG with β -actin as the loading control in uMDSCs^{MACS} of four groups were presented through bar graphs; (C) representative Western blot results of MHC and MyoG of all four groups in uMDSCs^{PP}; (D) the expression level of MHC and MyoG with β -actin as the loading control in uMDSCs^{PP} of four groups were presented through bar graphs. *, $P < 0.05$. Ctrl, Control group; Ind, Induction group; MAP, microenergy acoustic pulses group; MHC, muscle heavy chain; MyoG, myogenin; uMDSCs, urethral striated muscle derived stem/progenitor cells; MACS, magnetic-activated cell sorting.

function of organs under normal and disease states. In traditional methods, such as IF, when tissue sections are analyzed under the microscope, only short fragments of axons are observed in each section, and the 3D information of axonal structure is lost. Therefore, it is impossible for traditional methods to obtain a 3D picture of structural components or to describe the distribution of cells within tissues. The development of fluorescent proteins and laser scanning microscopy techniques which achieve deep tissue imaging of fluorescently labeled tissues along with the application of tissue clearing methods have opened new venues for the 3D imaging of tissues. Ertürk *et al.* (16) developed a highly reproducible and versatile clearing procedure called 3DISCO, which is applicable to diverse tissues including brain, spinal cord, immune organs, and tumors. 3DISCO is a powerful technique that offers 3D histological views of tissues in a fraction of the time and with a fraction of the labor required to complete standard histology studies. With this in mind, we first obtained 3D images of the whole female rat urethra. The images clearly reveal the distribution of urethral striated muscles and urethral smooth muscles from the bladder neck to the vaginal wall. Moreover, the images prove that the external

urethral sphincter (EUS) is located at the proximal urethra as has been previously reported (26). The images also demonstrate that there is a significant increase in striated muscle fibers in the EUS area, which is consistent with our previous report and Kim *et al.* (25,27).

To further support the localization of urethral striated muscle in the EUS, we also obtained IF images. From the cross-section of mid-urethra and the longitudinal rear urethral wall, we can differentiate the inner longitudinal smooth muscle layer, the middle circular smooth muscle layer, and the outer striated muscle layer, which together form the “smooth muscle-striated muscle zone”. The striated component of the urethral sphincter is the result of migration of later somite mesoderm cells into the periurethral smooth muscle mesenchyme, and these stem cells may differentiate into striated myotubules (28). In this study, we successfully showed both the localization of the urethral striated muscle in the EUS and we described the distribution of the striated muscle and smooth muscle with tissue 3DISCO and IF.

After localization of the striated muscle in the female rat urethra, we then attempted to harvest and identify MDSCs from the urethra. Stem cells are classically defined by

their multipotent long-term proliferation and self-renewal capabilities. With this in mind, researchers are hopeful that stem-cell-based therapies may provide alternative therapeutic options for a multitude of diseases including musculoskeletal and hematopoietic conditions (20). Previous studies have reported that MDSCs can be isolated from the hind limb and may be used to treat erectile dysfunction and other conditions (29-32). Moreover, our group previously reported that uMDSCs can be obtained from the rat urethra (3). To further identify the uMDSCs, we tested classical markers including Pax7, Sox2 and Lin28. Satellite cells are quiescent, mononucleated, myogenic cells located between the basal lamina and sarcolemma of muscle fibers. These cells can be activated by injury or other stimuli (33). Therefore, satellite cells can exhibit two different states, quiescent and activated, and each state has specific markers. Pax7, a signal of MDSC commitment to the myogenic lineage, expresses continually in both states (34). To date, the transcription factor Pax7 is the most reliable marker known to identify satellite cells (35). In addition, our group also used Pax7 as a classical marker for uMDSCs (3). Sox2, a "founding member" of the Sox gene family, is expressed in functionally defined neural stem cells and is a requirement in the maintenance of neural stem cells (23,36). Lin28, an evolutionarily conserved RNA-binding protein, is highly expressed in human and mouse embryonic stem cells (24). Yu *et al.* reported that Sox2 and Lin28 are sufficient to reprogram human somatic cells to pluripotent stem cells that exhibit the essential characteristics of stem cells (37). No previous study has investigated the use of these markers to identify uMDSCs. In the present study, we found Pax7 was positive to identify uMDSCs. Moreover, Sox2 and Lin28 were also positive for uMDSCs, suggesting that they also can be used as uMDSCs markers in the future studies.

To obtain the uMDSCs from the female rat urethra, we used two different methods: pre-plating and MACS. Pre-plating purification is an easy and efficient method based on the different cellular adherence rates and does not require special equipment (18,38), and MACS method is based on the previous report (39). In our experiment, we obtained uMDSCs with both methods and then compared cell proliferation between the methods. As shown in the *Figure 2B*, more uMDSCs were obtained with MACS compared to pre-plating using the same weight of urethral tissue. The cell count experiment corroborated these results. We then compared the cell proliferation of uMDSCs^{MACS} and uMDSCs^{PP}, and MACS demonstrated higher cell proliferation than pre-plating method. There

was a higher percentage of EdU, higher cell proliferation at different time points, higher overall cell proliferation rate, and shorter cell doubling time in uMDSCs^{MACS} as compared to uMDSCs^{PP}. These data suggest that MACS may be a better method of uMDSCs purification than pre-plating.

To further identify the uMDSCs and compare the two methods, we performed FACS assay. Previous authors reported that Pax7, Myf5, and MyoD were all positive in activated satellite cells while Myf5 and MyoD were both negative in quiescent satellite cells (40). In the present study, there were more Myf 5 (56.65%), CD34 (14.2%), and CD105 (0.135%) in uMDSCs^{MACS} than in uMDSCs^{PP} [Myf 5 (40.85%), CD34 (11.4%), and CD105 (0.06%), respectively].

Satellite cells differentiate into myogenic progenitor cells, or myoblasts, a committed muscle precursor. Myoblasts are highly proliferative and can further differentiate into myotubes to sustain muscle regeneration (41). With the aim to test the uMDSCs differentiation function, we performed a myotube formation experiment using uMDSCs. As reported in our previous study, L6 cells (immortalized rat skeletal myoblast cells) which can be purchased from commercial sources, can be induced with induction medium and MAP to form myotubes (3). MAP has attracted more and more attention over the past 40 years (42) and has been used to activate local stem/progenitor cells for the treatment of various urologic disorders including erectile dysfunction and UI (43,44). However, whether uMDSCs can be induced with MAP to form myotubes is far from clearly understood. In the present study, the longer myotube length, the larger myotube area, and the more nuclei number per myotube in Ind and MAP group compared to the Ctrl group suggested that uMDSCs can serve as stem cells to form myotubes. Moreover, we found that induction medium and MAP promote each other, with the longest myotube length, the largest myotube area, and the most nuclei per myotube in the Ind + MAP group. In addition, the enhanced expression of MHC and MyoG in Ind, MAP, and Ind + MAP groups versus the Ctrl group further supports the IF result. We conclude from this experiment that uMDSCs can serve as stem cells and differentiate into myotubes. The functional study of uMDSCs suggests that uMDSCs may be a potential therapeutic option for the treatment of SUI in the future and that induction medium and MAP have a cooperative effect on myotube formation.

In the present study, we successfully located and identified the striated muscle stem/progenitor cells in the female rat urethra. We then isolated the uMDSCs from the female rat urethra with MACS and pre-plating methods. Next, we

verified that the uMDSCs can be used as muscle stem cells to form myotubes and showed that induction medium and MAP can promote myotube formation. Finally, we used 3DISCO to describe the distribution of female rat urethral striated muscle and reported a more effective method to isolate uMDSCs. In the future, uMDSCs may serve as a treatment option for female SUI, and we hope that our findings can help to accelerate additional research efforts.

Acknowledgments

Funding: Research reported in this publication was supported by NIDDK of the National Institutes of Health under award number R56DK105097 and 1R01DK105097-01A1. It was also supported by Army, Navy, NIH, Air Force, VA and Health Affairs to support the AFIRM II effort, under Award number W81XWH-13-2-0052. Opinions, interpretations, conclusions and recommendations are those of the author and are not necessarily endorsed by the Department of Defense and do not necessarily represent the official views of the National Institutes of Health. This work is supported in part by the National Major Scientific and Technological Special Project for Significant New Drugs Development 2017ZX09304030 and China Scholarship Council under the Grant CSC201706160093.

Footnote

Conflicts of Interest: Tom F. Lue is consultant of AWCT, Inc. The other authors have no conflicts of interest to declare.

Ethical Statement: The authors are accountable for all aspects of the work in ensuring that questions related to the accuracy or integrity of any part of the work are appropriately investigated and resolved. The study was approved by the Institutional Animal Care and Use Committee of University of California, San Francisco (AN144689).

References

- Melville JL, Katon W, Delaney K, et al. Urinary incontinence in US women: a population-based study. *Arch Intern Med* 2005;165:537-42.
- Demaagd GA, Davenport TC. Management of urinary incontinence. *P T* 2012;37:345-61H.
- Wang B, Zhou J, Banie L, et al. Low-intensity extracorporeal shock wave therapy promotes myogenesis through PERK/ATF4 pathway. *Neurourol Urodyn* 2018;37:699-707.
- Wallner C, Dabhoiwala NE, DeRuiter MC, et al. The anatomical components of urinary continence. *Eur Urol* 2009;55:932-43.
- Ashton-Miller JA, Howard D, DeLancey JO. The functional anatomy of the female pelvic floor and stress continence control system. *Scand J Urol Nephrol Suppl* 2001;(207):1-7; discussion 106-25.
- Wang Z, Wen Y, Li YH, et al. Smooth Muscle Precursor Cells Derived from Human Pluripotent Stem Cells for Treatment of Stress Urinary Incontinence. *Stem Cells Dev* 2016;25:453-61.
- Turco MP, de Souza AB, de Campos Sousa I, et al. Periurethral muscle-derived mononuclear cell injection improves urethral sphincter restoration in rats. *Neurourol Urodyn* 2017;36:2011-8.
- Gilchrist AS, Rovner ES. Managing complications of slings. *Curr Opin Urol* 2011;21:291-6.
- Xu Y, Song YF, Lin ZX. Transplantation of muscle-derived stem cells plus biodegradable fibrin glue restores the urethral sphincter in a pudendal nerve-transected rat model. *Brazilian Journal of Medical and Biological Research* 2010;43:1076-83.
- Lin G, Wang G, Banie L, et al. Treatment of stress urinary incontinence with adipose tissue-derived stem cells. *Cytotherapy* 2010;12:88-95.
- Kinebuchi Y, Aizawa N, Imamura T, et al. Autologous bone-marrow-derived mesenchymal stem cell transplantation into injured rat urethral sphincter. *Int J Urol* 2010;17:359-68.
- Lim JJ, Jang JB, Kim JY, et al. Human umbilical cord blood mononuclear cell transplantation in rats with intrinsic sphincter deficiency. *J Korean Med Sci* 2010;25:663-70.
- Chargé SB, Rudnicki MA. Cellular and molecular regulation of muscle regeneration. *Physiol Rev* 2004;84:209-38.
- Ioppolo F, Rompe JD, Furia JP, et al. Clinical application of shock wave therapy (SWT) in musculoskeletal disorders. *Eur J Phys Rehabil Med* 2014;50:217-30.
- Zissler A, Steinbacher P, Zimmermann R, et al. Extracorporeal Shock Wave Therapy Accelerates Regeneration After Acute Skeletal Muscle Injury. *Am J Sports Med* 2017;45:676-84.
- Ertürk A, Becker K, Jährling N, et al. Three-dimensional imaging of solvent-cleared organs using 3DISCO. *Nat Protoc* 2012;7:1983-95.
- Breyer BN, Fandel TM, Alwaal A, et al. Comparison of spinal cord contusion and transection: functional and histological changes in the rat urinary bladder. *BJU Int* 2017;119:333-41.

18. Gong SP, Lee ST, Lee EJ, et al. Embryonic stem cell-like cells established by culture of adult ovarian cells in mice. *Fertil Steril* 2010;93:2594-601, 2601.e1-9.
19. Lin G, Garcia M, Ning H, et al. Defining stem and progenitor cells within adipose tissue. *Stem Cells Dev* 2008;17:1053-63.
20. Wu X, Wang S, Chen B, et al. Muscle-derived stem cells: isolation, characterization, differentiation, and application in cell and gene therapy. *Cell Tissue Res* 2010;340:549-67.
21. Deasy BM, Jankowski RJ, Huard J. Muscle-derived stem cells: characterization and potential for cell-mediated therapy. *Blood Cells Mol Dis* 2001;27:924-33.
22. Wu AK, Zhang X, Wang J, et al. Treatment of stress urinary incontinence with low-intensity extracorporeal shock wave therapy in a vaginal balloon dilation induced rat model. *Transl Androl Urol* 2018;7:S7-16.
23. Pevny LH, Nicolis SK. Sox2 roles in neural stem cells. *Int J Biochem Cell Biol* 2010;42:421-4.
24. Qiu C, Ma Y, Wang J, et al. Lin28-mediated post-transcriptional regulation of Oct4 expression in human embryonic stem cells. *Nucleic Acids Res* 2010;38:1240-8.
25. Zhang X, Alwaal A, Lin G, et al. Urethral musculature and innervation in the female rat. *NeuroUrol Urodyn* 2016;35:382-9.
26. Lim SH, Wang TJ, Tseng GF, et al. The distribution of muscles fibers and their types in the female rat urethra: cytoarchitecture and three-dimensional reconstruction. *Anat Rec (Hoboken)* 2013;296:1640-9.
27. Kim RJ, Kerns JM, Liu S, et al. Striated muscle and nerve fascicle distribution in the female rat urethral sphincter. *Anat Rec (Hoboken)* 2007;290:145-54.
28. Sarig R, Baruchi Z, Fuchs O, et al. Regeneration and transdifferentiation potential of muscle-derived stem cells propagated as myospheres. *Stem Cells* 2006;24:1769-78.
29. Kovanecz I, Vernet D, Masouminia M, et al. Implanted Muscle-Derived Stem Cells Ameliorate Erectile Dysfunction in a Rat Model of Type 2 Diabetes, but Their Repair Capacity Is Impaired by Their Prior Exposure to the Diabetic Milieu. *J Sex Med* 2016;13:786-97.
30. Kovanecz I, Rivera S, Nolzco G, et al. Separate or combined treatments with daily sildenafil, molsidomine, or muscle-derived stem cells prevent erectile dysfunction in a rat model of cavernosal nerve damage. *J Sex Med* 2012;9:2814-26.
31. Nolzco G, Kovanecz I, Vernet D, et al. Effect of muscle-derived stem cells on the restoration of corpora cavernosa smooth muscle and erectile function in the aged rat. *BJU Int* 2008;101:1156-64.
32. Wang JS, Kovanecz I, Vernet D, et al. Effects of sildenafil and/or muscle derived stem cells on myocardial infarction. *J Transl Med* 2012;10:159.
33. Bentzinger CF, Wang YX, Dumont NA, et al. Cellular dynamics in the muscle satellite cell niche. *EMBO Rep* 2013;14:1062-72.
34. Urish K, Kanda Y, Huard J. Initial failure in myoblast transplantation therapy has led the way toward the isolation of muscle stem cells: potential for tissue regeneration. *Curr Top Dev Biol* 2005;68:263-80.
35. Seale P, Sabourin LA, Girgis-Gabardo A, et al. Pax7 is required for the specification of myogenic satellite cells. *Cell* 2000;102:777-86.
36. Graham V, Khudyakov J, Ellis P, et al. SOX2 Functions to Maintain Neural Progenitor Identity. *Neuron* 2003;39:749-65.
37. Yu J, Vodyanik MA, Smuga-Otto K, et al. Induced pluripotent stem cell lines derived from human somatic cells. *Science* 2007;318:1917-20.
38. Khosravi-Farsani S, Amidi F, Habibi Roudkenar M, et al. Isolation and enrichment of mouse female germ line stem cells. *Cell J* 2015;16:406-15.
39. Sacco A, Doyonnas R, Kraft P, et al. Self-renewal and expansion of single transplanted muscle stem cells. *Nature* 2008;456:502-6.
40. Fujimaki S, Hidaka R, Asashima M, et al. Wnt protein-mediated satellite cell conversion in adult and aged mice following voluntary wheel running. *J Biol Chem* 2014;289:7399-412.
41. Chang NC, Rudnicki MA. Satellite cells: the architects of skeletal muscle. *Curr Top Dev Biol* 2014;107:161-81.
42. Haupt G. Use of extracorporeal shock waves in the treatment of pseudarthrosis, tendinopathy and other orthopedic diseases. *J Urol* 1997;158:4-11.
43. Ruan Y, Zhou J, Kang N, et al. The effect of low-intensity extracorporeal shockwave therapy in an obesity-associated erectile dysfunction rat model. *BJU Int* 2018;122:133-42.
44. Wang HS, Oh BS, Wang B, et al. Low-intensity extracorporeal shockwave therapy ameliorates diabetic underactive bladder in streptozotocin-induced diabetic rats. *BJU Int* 2018;122:490-500.

Cite this article as: Cui K, Kang N, Banie L, Zhou T, Liu T, Wang B, Ruan Y, Peng D, Wang HS, Wang T, Wang G, Reed-Maldonado AB, Chen Z, Lin G, Lue TF. Microenergy acoustic pulses induced myogenesis of urethral striated muscle stem/progenitor cells. *Transl Androl Urol* 2019;8(5):489-500. doi: 10.21037/tau.2019.08.18

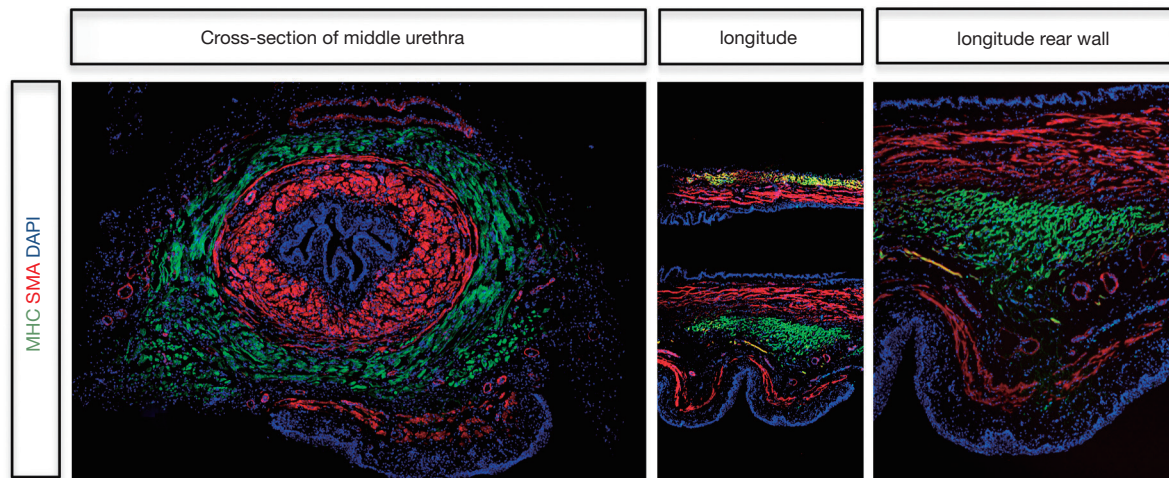


Figure S1 Localization of urethral striated muscle in external urethral sphincter. The IF images of the cross-section of middle urethra, a longitudinal section of urethra, and a longitudinal section of the posterior urethral wall stained with SMA (red) and MHC (green). SMA, smooth muscle actin; MHC, muscle heavy chain; DAPI, 4',6-diamidino-2-phenylindole.

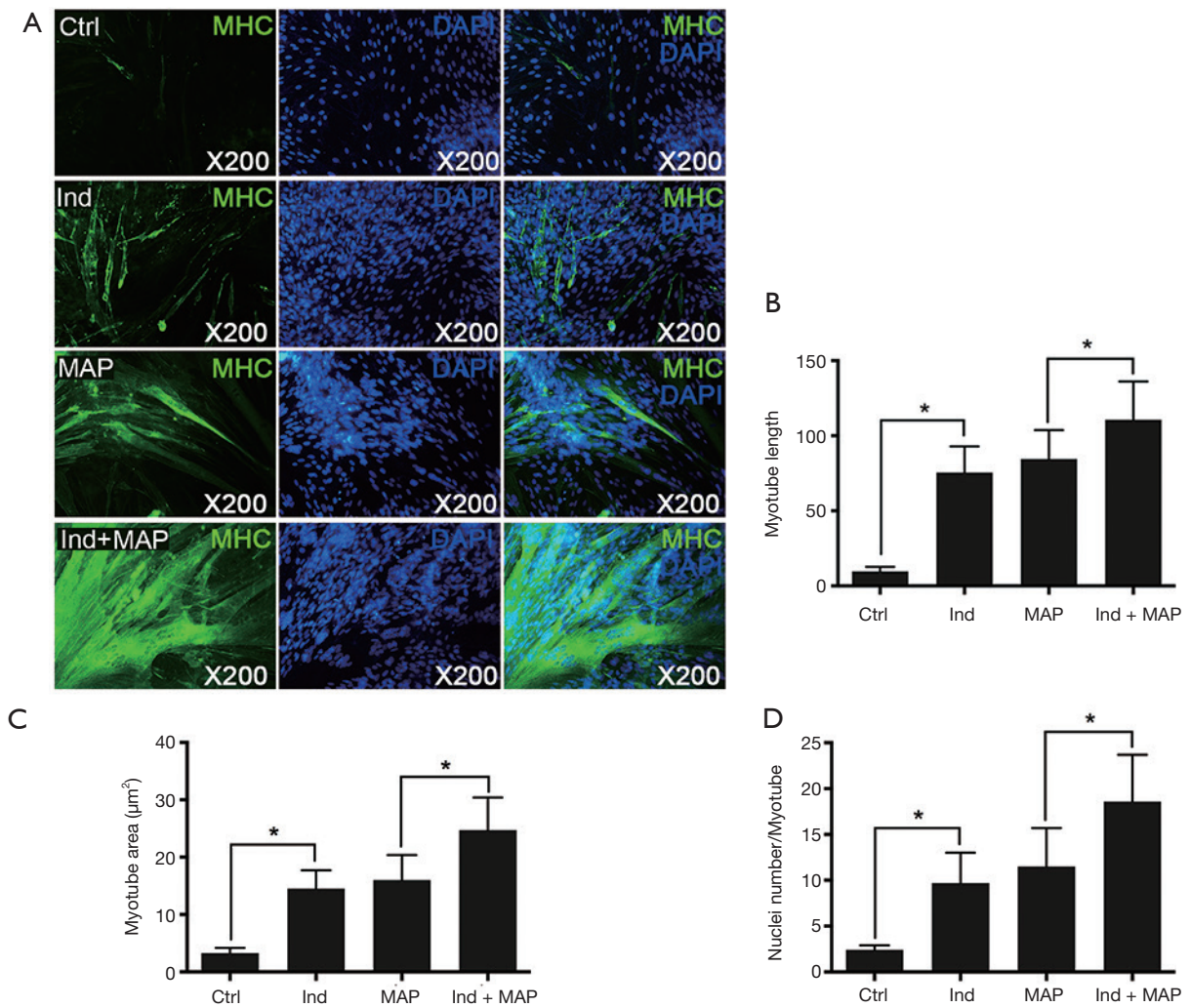


Figure S2 Myotube formation of L6 cells through Western blot. (A) Representative western blot results of MHC and MyoG of all four groups in L6 cells; $\times 200$. (B) the expression level of MHC and MyoG with β -actin as the loading control in L6 cells of four groups were presented through bar graphs; (C) myotube area; (D) cell nuclei number in each myotube. *, $P < 0.05$. Ctrl, Control group; Ind, Induction group; MAP, microenergy acoustic pulses group; MHC, muscle heavy chain; DAPI, 4',6-diamidino-2-phenylindole; MyoG, myogenin.